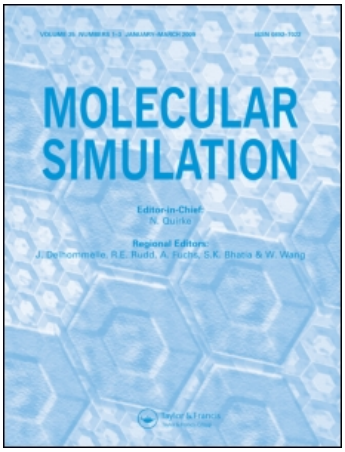

Molecular Simulation
Publication details, including instructions for authors and subscription information:
http://www.informaworld.com/smpp/title~content=t713644482

Theoretical study of the mechanism behind the *para*-selective nitration of toluene in zeolite H-Beta

Amity Andersen[a]; Niranjan Govind[b]; Lalitha Subramanian[a]
[a] Accelrys, Inc., San Diego, CA, USA [b] William R. Wiley Environmental Molecular Sciences Laboratory, Pacific Northwest National Laboratory, Richland, WA, USA

To cite this Article Andersen, Amity , Govind, Niranjan and Subramanian, Lalitha(2008) 'Theoretical study of the mechanism behind the *para*-selective nitration of toluene in zeolite H-Beta', Molecular Simulation, 34: 10, 1025 — 1039
To link to this Article: DOI: 10.1080/08927020802191958
URL: http://dx.doi.org/10.1080/08927020802191958

Molecular Simulation
Vol. 34, Nos. 10–15, September–December 2008, 1025–1039

Taylor & Francis
Taylor & Francis Group

Theoretical study of the mechanism behind the *para*-selective nitration of toluene in zeolite H-Beta

Amity Andersen[a]*, Niranjan Govind[b]* and Lalitha Subramanian[a]

[a]*Accelrys, Inc., San Diego, CA, USA;* [b]*William R. Wiley Environmental Molecular Sciences Laboratory, Pacific Northwest National Laboratory, Richland, WA, USA*

(*Received 30 January 2008; final version received 9 May 2008*)

Periodic density functional theory calculations were performed to investigate the origin of the favourable *para*-selective nitration of toluene exhibited by zeolite H-beta with acetyl nitrate nitration agent. Energy calculations were performed for each of the 32 crystallographically unique Brønsted acid sites of a beta polymorph B zeolite unit cell with multiple Brønsted acid sites of comparable stability. However, one particular aluminum T-site with three favourable Brønsted site oxygens embedded in a straight 12-T channel wall provides multiple favourable proton transfer sites. Transition state searches around this aluminum site were performed to determine the barrier to reaction for both *para* and *ortho* nitration of toluene. A three-step process was assumed for the nitration of toluene with two organic intermediates: the π- and σ-complexes. The rate limiting step is the proton transfer from the σ-complex to a zeolite Brønsted site. The barrier for this step in *ortho* nitration is shown to be nearly 2.5 times that in *para* nitration. This discrepancy appears to be due to steric constraints imposed by the curvature of the large 12-T pore channels of beta and the toluene methyl group in the *ortho* approach that are not present in the *para* approach.

Keywords: toluene; nitration; beta; zeolite; density functional theory

1. Introduction

Nitration of aromatic compounds such as toluene are important for the synthesis of small-molecule precursors for further use in fine chemicals such as dyes, pharmaceuticals, perfumes, plastics and explosives [1–3]. Typically, it is the *para* nitration product of monosubstituted benzene compounds that is the most desirable [4]. The traditional aromatic nitration method that is still in wide use today is the homogeneous solution-phase catalysis of the aromatic compound by nitric acid species in a mixture of substrate, nitric acid and sulfuric acid [5]. However, the nitration of aromatics such as toluene is not very selective (toluene nitration of the *ortho*, *meta* and *para* is about 40, 3 and 57%, respectively [5]) and often leads to over-nitration and oxidised by products and the creation of environmentally unfriendly acid waste that is expensive to treat. More recently, a number of promising catalysts have been proposed as 'green' alternatives to the traditional method of nitration. These include lanthanide triflate [6], Nafion-H and other polysulfonic acid resins [7], bismuth subnitrate and thionyl chloride [8], montmorillonite clay-supported copper(II) nitrate [9] and various zeolites (e.g. mordenite [10], ZSM-11 [11], ZSM-5 [12], zeolite beta [4] and faujasite [13]).

Of these, the solid acid zeolites are among the most promising. The advantages of zeolites are the easy removal of substrate and product, regioselectivity, operation under relatively mild conditions and recyclability. The most promising zeolite for the *para*-selective nitration of toluene is H-beta zeolite. The suitability of H-beta as a selective toluene nitration catalyst was shown in the pioneering synthesis work of Smith et al. [4]. In their synthesis method, H-beta zeolite was first combined with concentrated nitric acid (90%) followed by acetic anhydride (Ac_2O) to effectively create acetyl nitrate and acetic acid. The acetic anhydride was also added in excess to undergo hydrolysis and effectively remove water molecules that may otherwise poison the acid sites of the H-beta. After adding acetic anhydride, toluene was then added to undergo nitration. The nitration of toluene was quantitative ($>99\%$), and the resulting nitration yielded up to 81% *para* nitrotoluene. Decreasing the temperature from 30 to 50°C resulted in a slight increase in *para* product. Having a stoichiometric ratio of Ac_2O to HNO_3 gave optimal *para* selectivity. Increasing the amount of beta zeolite with respect to the Ac_2O and HNO_3 reagents increased the *para* product. Vacuum distillation proved to be the best means of restoring H-beta to a near-pristine state after one round of toluene nitration. The recycled H-beta could undergo a few more rounds of toluene nitration before diminished nitration ability was seen. High *para* selectivity seemed to be unique to beta. Experiments with H-mordenite, H-ZSM-5 and H-Y did not yield as high a *para* selectivity as observed for H-beta [4].

*Corresponding authors. Emails: aandersen@accelrys.com; nirigovind@pnl.gov

ISSN 0892-7022 print/ISSN 1029-0435 online

DOI: 10.1080/08927020802191958
http://www.informaworld.com

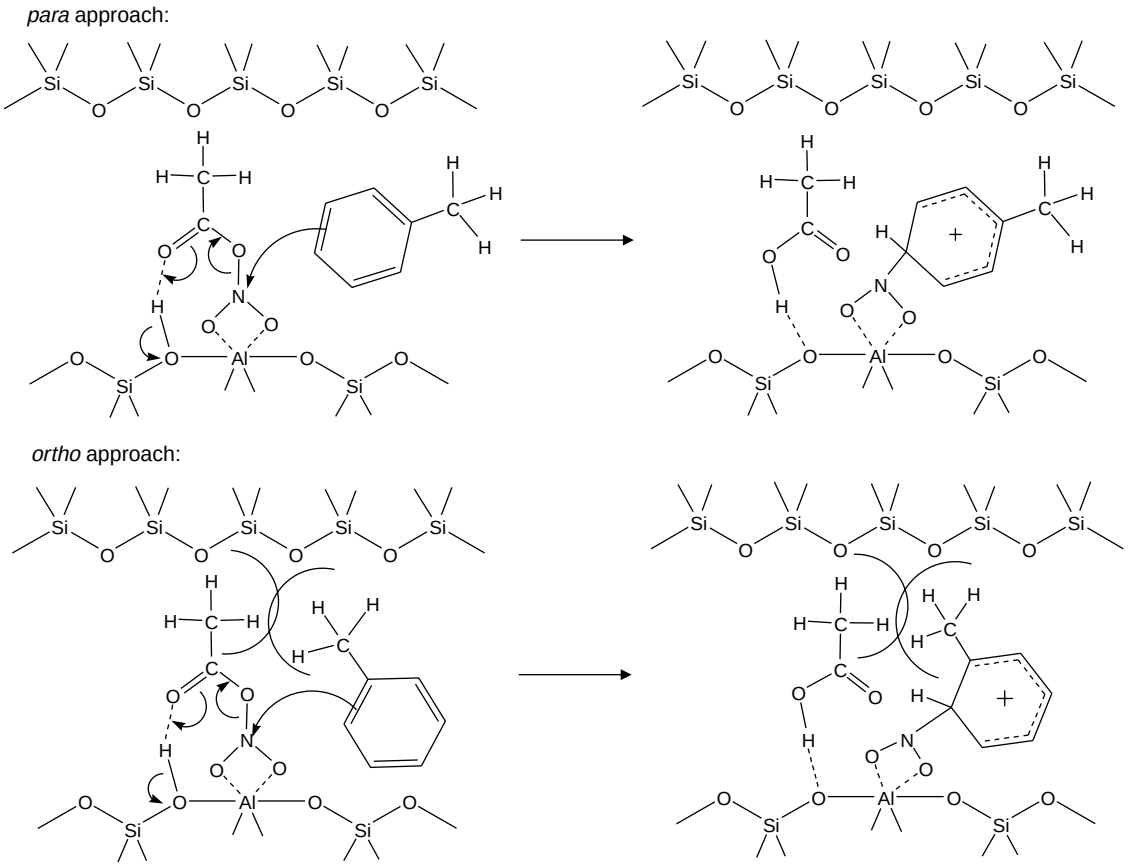

Figure 1. Scheme to explain favourable *para* nitration according to the work of Prins and coworkers [14,15]. Note that steric hindrance from the acetyl and toluene methyl group interaction is proposed to prevent toluene nitration in the *ortho* approach case.

Following the work of Smith et al., Prins and coworkers applied liquid and solid state MAS NMR to Ac_2O/HNO_3 liquid and in beta to try to elucidate the mechanism for beta zeolite's unique *para* selectivity [14–16]. Prins and coworkers suggested that the source of beta zeolites high selectivity toward *para*-selectivity was due to steric hindrance imposed by the acetyl group of acetyl nitrate bound to the octahedral (i.e. Lewis acid) aluminum sites of the zeolite cage via the nitrate group (this mechanism is depicted in Figure 1). However, this explanation of beta's selectivity is tentative, since they observed octahedral aluminum ^{27}Al MAS NMR nitrate peak disappearance upon the addition of acetic anhydride to the nitric acid treated beta zeolite. A broad octahedral aluminum peak persisted, but Prins and coworkers did not have definitive evidence that the octahedral peaks were due to acetyl nitrate binding or to other species binding such as acetic anhydride, acetic acid or residual nitrate. Some tetrahedral aluminum recovery was observed. Partial Al—O—Si hydrolysis has been proposed for the mechanism responsible for the appearance of octahedral aluminum in the steam treatment of beta and other zeolites and aluminosilicates [17–26]. Since acetic acid is able to donate another proton to a Al—O—Si linkage (as with nitric acid [18]), it seems that the acetate ion conjugate base would be a more appropriate species for octahedral coordination of aluminum compared to the acetyl nitrate molecule. Therefore, the origin of beta's unique *para* selectivity still has yet to be explained satisfactorily.

There is also a diffusional component to beta's *para* selectivity. Beta has a three-dimensional network of large 12-T pore channels (shown in the two polymorph structures of Figures 2 and 3), which are the most likely diffusion paths for large molecular species such as toluene and nitrotoluene. Such a network of large channels allow toluene reagent and nitrotoluene product to readily diffuse in and out of the beta zeolite structure. Selective nitration of toluene has been shown to occur in high surface area microcrystalline beta, not macrocrystalline beta [27]. This indicates that diffusion into the micropore system is required for selective *para* nitration to occur. A shape-selection explanation was also explored to explain the *para* selectivity, where the pore network allowed for excellent diffusion of reagents into the network and a possible restriction of *ortho* species diffusion out of the system. The *ortho* species have a geometry that may make their

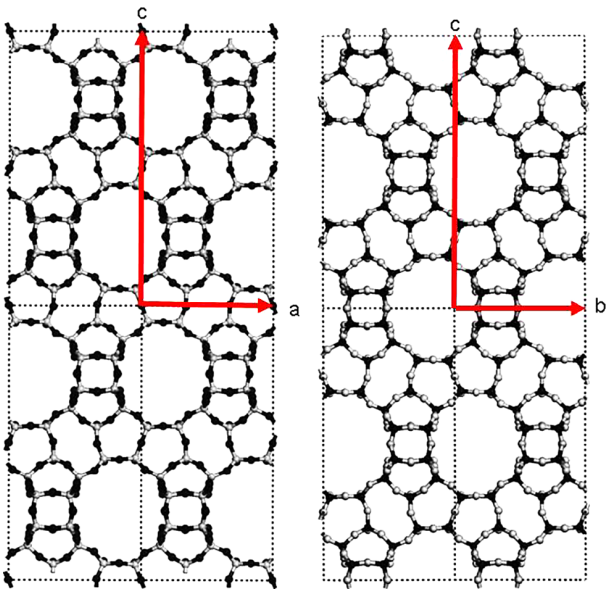

Figure 2. Polymorph A ac plane view (left). Polymorph A bc plane view (right). The dark balls are oxygen atoms, and the light balls are silicon atoms.

diffusion more restrictive. However, Smith and coworkers and Prins and coworkers reported almost quantitative recovery of the nitrotoluene product, regardless of the isomer shape. Thus, the *para* selectivity of beta zeolite seems to be an intrinsic property of this zeolite that is not completely explained by diffusion properties. Other zeolites with large 12-T channel 'plumbing' (e.g. mordenite) do not show the same *para* selectivity that beta exhibits. It is the aim of this study to provide in-depth mechanistic details of *para* nitration of toluene by *in situ* acetyl nitrate in H-beta zeolite via atomistic and electronic structure insight.

2. Theoretical method

2.1 Density functional theory calculations

All-electron periodic density functional theory (DFT) calculations were performed using the commercial version (Accelrys' Materials Studio® 4.0, San Diego, CA, USA, [28]) of DMol^3, [29,30]. The generalised gradient approximation exchange-correlation functional of Perdew, Burke and Ernzerhof was used for all DFT calculations [31]. All calculations employed the double numerical local atomic basis set including a polarisation d-function on all non-hydrogen atoms and a polarisation p-function on all hydrogen atoms. The atomic radius cut-off was set at 4.2 Å. Since the zeolite models considered here are large (>96 atoms), calculations at the Γ-point were sufficient. The energy convergence tolerance was set to 1×10^{-5} Hartree. The geometry convergence tolerance was set to 2×10^{-5} Hartree, and the force and displacement convergence thresholds were set to 4×10^{-3} Hartree/Å and 5×10^{-3} Å, respectively. Thermal smearing was used to aid convergence and was set to 0.005 Hartree. The delocalised internal option was invoked for geometry optimisation [32]. For transition state searches along proposed reaction pathways, the generalised synchronous transit approach was used to locate saddle points along a path anchored by reactant and product minima [33].

2.2 Structure of beta zeolite

Pure silica and aluminosilicate beta zeolite consists of an intergrowth of two polymorphs, A and B, having

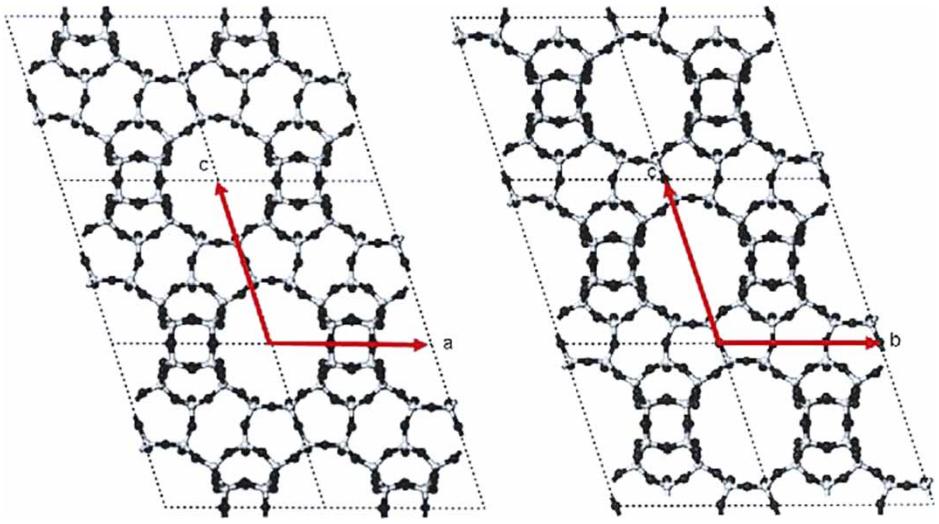

Figure 3. Polymorph B ac plane view (left). Polymorph B bc plane view (right). The dark balls are oxygen atoms, and the light balls are silicon atoms.

approximately, a 40:60 ratio of the two polymorphs [34]. The ratio of A and B polymorphs can vary with crystallite size [35]. Figure 2 shows the structure of polymorph A, and Figure 3 shows the structure of polymorph B. The polymorphs of beta differ primarily in the stacking of tertiary building units in the *z*-direction. Polymorph A is characterised as a racemic mixture of two enantiomeric structures, having either left or right helical stacking of building units at the (001) plane about a four-fold screw axis. The enantiomeric space group pair for polymorph A is $P4_122$ and $P4_322$. On the other hand, polymorph B is achiral in character and has the space group $C2/c$. Newsam et al. also described a hypothetical polymorph C with higher symmetry (space group $P42/mmc$), which is not found in the pure silica and aluminosilicate varieties of beta zeolite [34]. However, germanosilicate varieties of beta zeolite bearing the polymorph C structure have been synthesised recently [36]. Interestingly, the disordered stacking sequences of the polymorphs do not greatly affect the accessible pore volume. However, the stacking disorder greatly determines the tortuosity of the 12-T pore system along the *z*-direction [34]. Incidentally, stacking faults can occur at the (001) stacking plane, creating Lewis acid type undercoordinated aluminum sites and silanol functionality [37].

In this work, we chose to use the beta primitive polymorph B cell lattice in all our calculations. The primitive cell of pure silica beta polymorph B has 96 atoms, which is a little less than half the size of the cell lattice of pure silica polymorph A (206 atoms). Thus, the beta polymorph B model is the least expensive beta model from a computational standpoint. Moreover, polymorph B tends to be present in slightly higher amounts compared with polymorph A (polymorph B being about 62.5%) [34]. The lattice parameters of the primitive monoclinic beta polymorph B cell are $a = b = 12.66$ Å, $c = 14.33$ Å, $\alpha = \beta = 107.24^\circ$ and $\gamma = 90.06^\circ$ (constructed from the conventional cell described in Newsam et al. [34]). These cell parameters were held fixed during structure optimisation, but the atom positions were allowed to relax.

2.3 Location of Brønsted acid sites

The approach for studying the Brønsted acid sites in H-beta is similar to that of Hill et al. [38] and Govind et al. [39]. For polymorph B of beta zeolite, one silicon atom in a pure silica beta B model was replaced with an aluminum atom and the resulting positive charge deficit was compensated with a proton at one of the oxygen atoms coordinating the aluminum to ensure neutrality. This protocol was repeated for all crystallographically unique Brønsted acid sites in the original pure silica beta B model. According to the original paper by Newsam et al. detailing the structure of beta zeolite, all polymorphs of pure silica beta have nine

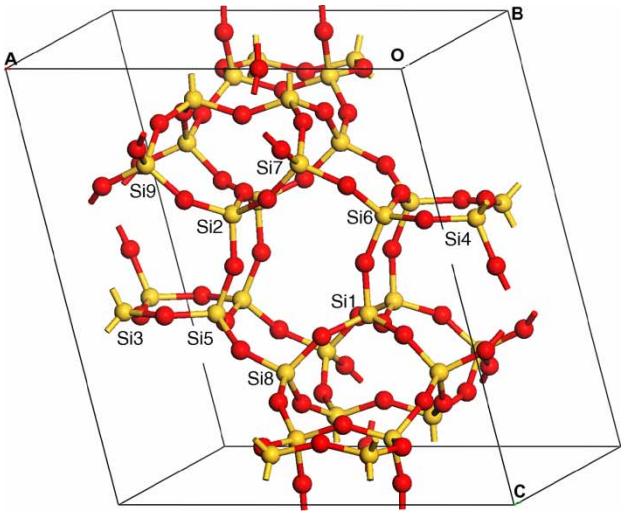

Figure 4. The nine crystallographically unique silicon atoms of beta polymorph B. Note atom assignments in beta polymorph A are similar.

crystallographically unique silicon atoms [34]. These nine silicon atoms have been labelled in the beta polymorph B structure shown in Figure 4. Since each silicon is coordinated by four oxygen atoms, there are $9 \times 4 = 36$ possible Brønsted acid sites. However, the silicon atoms labelled with numbers 8 and 9 in the work of Newsam et al. have only two unique oxygen atoms [34]. Thus, there are only 32 unique Brønsted acid sites. All 32 of these Brønsted acid site beta structures were optimised with DFT as detailed in the electronic structure section described earlier. Relative energies for the optimised 32 structures were established based on the total energy of the optimised structure bearing the lowest total energy.

2.4 Nitration of toluene by acetyl nitrate and the beta Brønsted acid site

Once a likely Brønsted acid site was determined from the above protocol, a number of acetyl nitrate orientations around the acid site were generated and optimised. The lowest energy orientation was chosen to study the reaction of acetyl nitrate with toluene. The toluene was placed close to the acetyl nitrate NO_2 moiety for two scenarios: electrophilic *para* attack and electrophilic *ortho* attack. The H-beta zeolite, acetyl nitrate and toluene models were then optimised to give the 'reactant' minima for subsequent transition state searches. The mechanism for the reactant, intermediate and product minima and transition states for *para* and *ortho* toluene nitration were partially inspired by the mechanistic work of Olah and coworkers [1,40] and the work of Silva and Nascimento [41] for the nitration of benzene in the gas phase and via formyl nitrate and a 5-T (pentameric) cluster

carved from beta zeolite, respectively. From these minima, the appropriate transition states were found using the transition state algorithm described earlier to build potential energy profiles for the nitration of toluene by acetyl nitrate in the presence of the beta acid site catalyst.

3. Results and discussion

3.1 Aluminum and Brønsted acid sites

Table 1 lists the relative energies based on our calculated DFT total energies for the 32 crystallographically unique Brønsted acid sites. The distribution of relative energies is fairly narrow (6.0 ± 3.5 kcal/mol), but a little wider than the 1.4 kcal/mol range previously reported by Pápai et al. from DFT calculations on pentameric cluster models [42]. Despite the location of the Brønsted acid site in a strained 4-T ring, the Al1–O3 acid site appears to be the most stable of the acid sites (see Figure 5 for an illustration of this site). Moreover, it is interesting that all four coordinated oxygen atoms around the Al1 site have fairly low energies relative to Al1–O3. The Al1–O2 site is only 2.0 kcal/mol higher than the Al1–O3 site. This is an important feature of this site, which will be explored shortly in the reaction mechanism proposed for nitration of toluene. Note also that much of the stability of site Al1–O3 and site Al–O2 is due to the noticeable intra-cage hydrogen bonding. These Brønsted acid sites are similar to the lowest energy sites Fujita et al. have found in the oval-shaped 6-T rings of polymorph A using electronic structure methods [43].

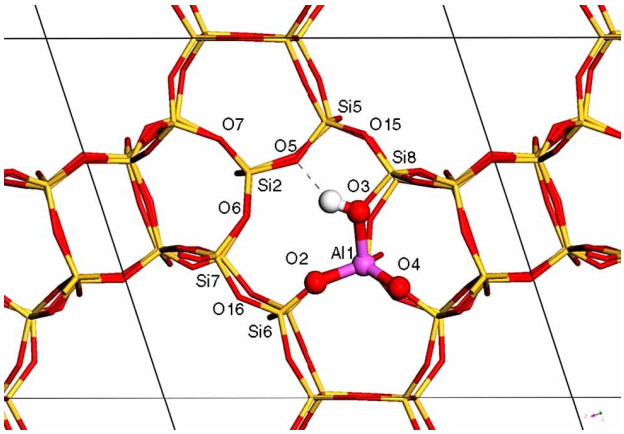

Figure 5. The most stable Brønsted acid site (Al1–O3) for the beta polymorph B system. Note that Al1–O2 and Al1–O4 are also relatively low in energy (2.0 and 4.1 kcal/mol, respectively).

Table 1. Brønsted acid site energies (in kcal/mol) for all possible sites in beta B polymorph.

Aluminum site[a]	Brønsted site[a]	Relative energy[b]
Al1	O1	5.8
	O2	2.0
	O3	0.0
	O4	4.1
Al2	O1	10.0
	O5	3.5
	O6	4.1
	O7	5.7
Al3	O8	6.2
	O9	5.0
	O10	7.4
	O11	5.6
Al4	O8	4.1
	O11	2.2
	O12	5.4
	O13	6.7
Al5	O5	3.9
	O9	6.6
	O14	5.1
	O15	10.6
Al6	O2	3.1
	O12	6.0
	O14	3.6
	O16	9.5
Al7	O4	12.4
	O6	3.8
	O10	4.0
	O16	7.9
Al8	O3	2.9
	O15	5.6
Al9	O7	15.0
	O13	7.3

[a] Numbering based on crystallographic ordering specified by Newsam et al. [34]. [b] Relative energy with respect to the lowest energy site found in this study (in this case, Al1–O3).

Though nine unique silicon sites can be discerned from Fyfe et al.'s ^{29}Si MAS NMR spectra for highly siliceous beta, the conspicuous trimodal character of these spectra suggests that these nine unique silicon sites can be classified into three general categories [44]. An in-depth theoretical analysis of Fyfe et al.'s early findings was performed by Valerio et al. using SOS–DPFT to simulate nuclear magnetic resonance shifts [45]. Their assumption of three primary categories for the nine unique Al site types based on inclusion/exclusion of the Al sites in 4-T rings (i.e. whether the Al is included in two, one or zero 4-T rings) proved to agree well with experiment. From their work it was found that sites 3–6 comprise the group of T sites contained in two 4-T ring systems. Sites 7–9 comprise the group of T sites not contained in any 4-T ring system. Finally, sites 1 and 2 comprise the group of T sites contained in only one 4-T ring moiety. Van Bokhoven et al. have done further ^{27}Al MAS NMR studies of beta zeolite undergoing steam dealumination and found that sites 1 and 2 sites are the most stable aluminum sites in the structure, resisting dealumination up to 600°C [17]. Moreover, they found that all sites but sites 1 and 2 can readily undergo a tetrahedral to octahedral coordination change under steam

conditions. This change in coordination is reversible under mild steaming conditions. This octahedral aluminum coordination has also been observed in the addition of concentrated nitric acid to beta zeolite, the first step in the synthesis of nitrotoluene in beta [14,18,27].

Abraham et al.'s experimental ^{27}Al MAS NMR work on stepwise calcined H-beta [19] has shown Si/Al ratio dependence for Al site occupation, suggesting a potential non-random process for Al site selection (likely due to the crystallisation kinetics process). Their experiments also suggest that two adjacent Al sites (obeying Löwenstein's rule of no Al—O—Al linkages [46]) are required for the hydrolysis of Al—O—Si linkages and, therefore, octahedral coordination of Al sites. Our results for aluminum site occupation in our model H-beta system agrees with Abraham et al.'s observation that, for high Si/Al ratio (i.e. Si/Al = 110 and 215) or extremely low aluminum content, octahedral aluminum sites are absent. That is, the most stable aluminum sites will tend to be sites 1 and 2, which do not demonstrate an octahedral coordination shift of the aluminum upon calcination, steaming or, in the case of aromatic nitration, nitric acid treatment. However, the lack of octahedral species may also be due to a lack of close aluminum site pairs. The presence of aluminum acid site pairs in beta zeolite has also been proposed by Bortnovsky et al. based on FTIR spectroscopy with acetonitrile molecular probe experiments on Co^{2+}-exchanged beta [47]. Indeed, the presence of two close-by Al sites is an appealing zeolite feature for divalent transition metal exchange ions (which require a two-fold counter ion compensation) for NO_x selective catalytic reduction catalysts as explored recently in the theory works of Fujita et al. [43] and Fischer et al. [48].

Though aluminum site pairs like those seen in Abraham et al.'s work are likely to be prevalent with the Si/Al ≈ 13 beta used in the nitration experiments of Prins and coworkers [14,16,18,27] and Smith and coworkers [4], our proposed mechanism for the nitration of toluene with the acetyl nitrate nitration agent in H-beta depends on a single acid site. Though, our present mechanism adequately explains the basic mechanism for *para*-selective nitration, we are exploring the formation of the acetyl nitrate nitration agent and subsequent toluene nitration in an aluminum acid site pair model for an upcoming study [49].

3.2 *Adsorption of acetyl nitrate at Brønsted acid sites*

We first searched for a nitrate–aluminum bound acetyl nitrate structure as proposed by Prins and coworkers. Prins and coworkers have used chemical anisotropy broadening arguments in their ^{15}N NMR results to claim that the NO_2 moiety is bound to the aluminum site [14,18,27].

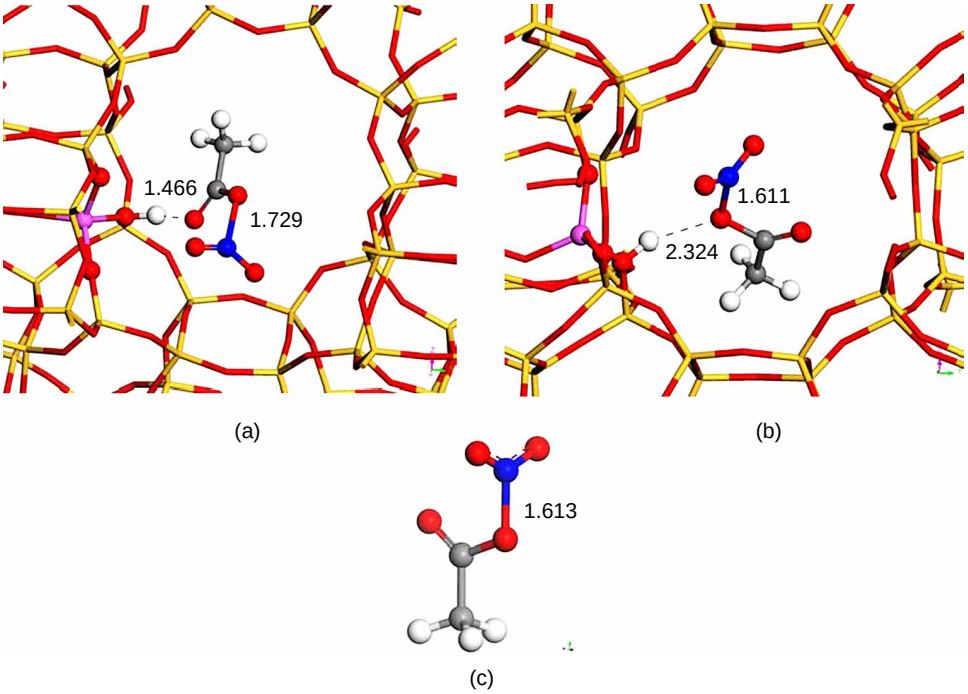

Figure 6. (a) Carbonyl oxygen hydrogen-bonding of acetyl nitrate, (b) ester linkage oxygen hydrogen-bonding of acetyl nitrate and (c) gas-phase acetyl nitrate. Distances and bond lengths are in Angstrom.

We, however, were unsuccessful in finding such a species with our Al1–O3 acid site model. As mentioned previously, Al sites 1 and 2 are not as flexible as Al sites 3–9, [19]. Thus, stable nitrate coordination with Al1 would not be expected. More of an interaction between the nitrate moiety of the acetyl nitrate and Al sites 3–9 may be possible since these sites participate in octahedral coordination because of their flexibility, which we are currently pursuing [49]. Prins and coworkers have noted that ZSM-5 also exhibits similar broadening, but octahedral aluminum coordination occurs negligibly in ZSM-5 [27]. Thus, there appears to be more than one-way to explain the broadening they observed. We show that chemical anisotropy (i.e. distortion of the nitrate moiety) can occur through means other than nitrate binding to Al. For the acetyl carbonyl oxygen binding at the proton site shown in Figure 6, the optimised structure shows a sizeable elongation of the N—O(ester linkage) bond (1.729 Å). The H-bonding of the zeolite cage proton and the carbonyl oxygen is short (1.466 Å). Both the long N—O(ester linkage) bond and the short H(cage)—O (carbonyl) H-bond suggest that this mode of acetyl nitrate binding is going to be most amenable to toluene nitration. That is, the N—O(ester linkage) will readily rupture to form a 'nitronium' moiety to attack toluene and the transfer of the cage proton to the acetyl carbonyl oxygen to form acetic acid will be facile.

We also considered the scenario, where the ester linkage oxygen of acetyl nitrate interacts with the proton site. This manner of acetyl nitrate interaction was considered in the mechanism proposed by Silva et al. for the nitration of benzene by formyl nitrate in their DFT calculation on a pentameric cluster model [41]. In this scenario, the distortion of the N—O(ester linkage) bond is not as pronounced (1.611 Å) and the H-bond between the ester linkage oxygen and the zeolite proton appears weaker (2.324 Å). Thus, the scenario involving the acetyl carbonyl interaction with the zeolite cage proton may be more in line with the observation of anisotropy. Moreover, this interaction scenario is the most stable from the total energy calculations performed here (by 10.1 kcal/mol).

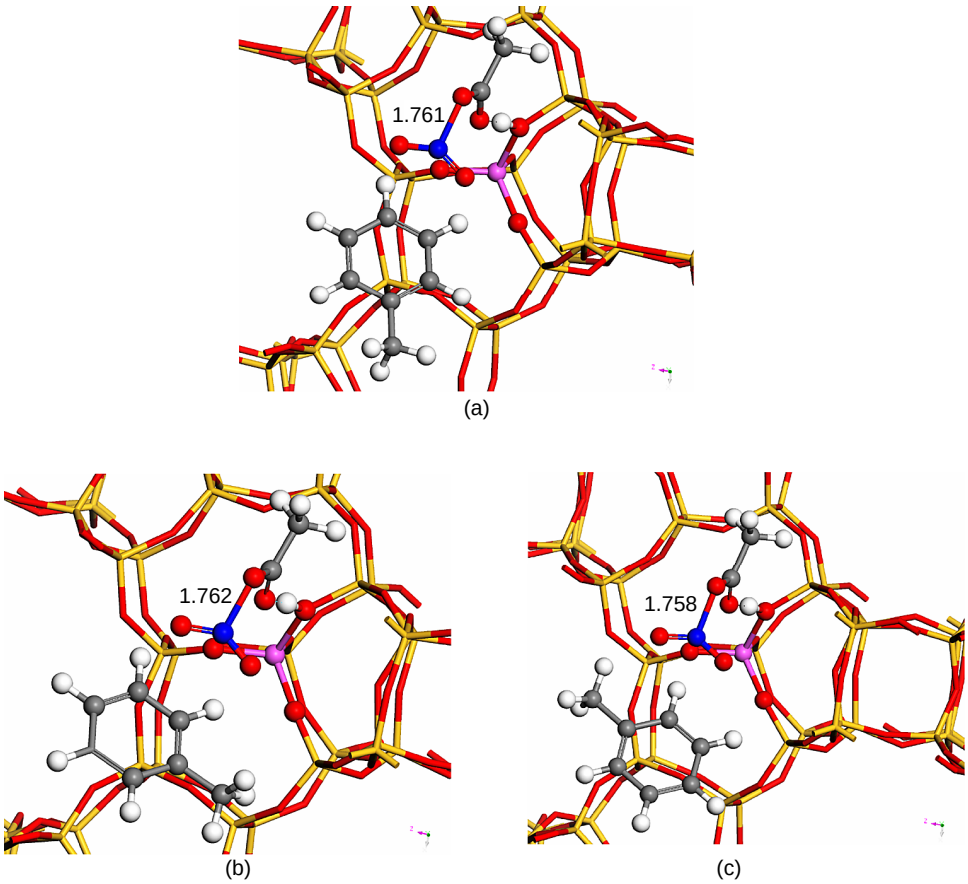

Figure 7. Reactant structures (acetyl nitrate and toluene) in side cross-section of 12-T pore around Brønsted acid site for (a) *para*, (b) *ortho* 1 and (c) *ortho* 2 attack orientations of toluene. Distance and bond lengths are in Angstrom.

3.3 Para *versus* ortho *nitration of toluene in beta*

Para and *ortho* nitration was considered around the Al1 site. As mentioned earlier, the three oxygens surrounding Al1 in the 12-T pore wall are the most stable Brønsted acid sites, with the Al1–O3 site being the lowest in energy. The Al1–O3 is assumed to be protonated at the beginning of the series of reactions leading to toluene nitration with the carbonyl oxygen of the acetyl nitrate hydrogen-bonding with the proton of the Al1–O3 site. However, there are likely to be other potential Brønsted acid sites. The calculations considered one *para* site and the two possible *ortho* sites on toluene. Figure 7 shows the starting point for the reactants, toluene and acetyl nitrate, in our calculations.

Nitration of the toluene appears to be a three-step process, demonstrated with DFT calculations of benzene nitration in the gas-phase by Olah and coworkers [40]. The acetyl nitrate readily transfers a 'nitronium'-like moiety to the π-system of the toluene close to the *para* or *ortho* sites. This is a π-complex with no real bonding interaction. A sp^2 to sp^3 hybridisation of the *para* or *ortho* carbon must then occur to create a σ-complex (a.k.a., Wheland intermediate or arenium cation). Finally, this σ-complex must transfer the proton from the *para* or *ortho* site to a Brønsted acid site in the zeolite wall. Upon optimising the H-beta structure with the acetyl nitrate site and toluene, it became clear that the most likely acid transfer site after creation of the σ-complex is the Al1–O2 site in our model, which, as we already mentioned previously, has comparable stability to Al1–O3. The presence of two nearby Brønsted acid sites that participate in the necessary proton transfer steps is an important feature of the selectivity mechanism of our model. A similar two oxygen with one aluminum acid site cluster model was proposed by Silva et al. in their mechanism for benzene nitration by formyl nitrate [41]. Two nearby Brønsted acid sites may be achieved with a nearby aluminum pair model (Al—O—Si—O—Al in accord with Löwenstein's rule). We are currently studying this model [49].

Figure 8 shows the reaction path for the nitration of toluene in the beta zeolite pore system and for the three-site nitration scenarios. Table 2 shows the energetics for the three reactions and the barriers to reaction. The energetics have not been corrected for temperature, zero point vibrational energies or solvent effects. However, such corrections are not expected to change the mechanistic message of our work. Figure 9 shows the structures of the

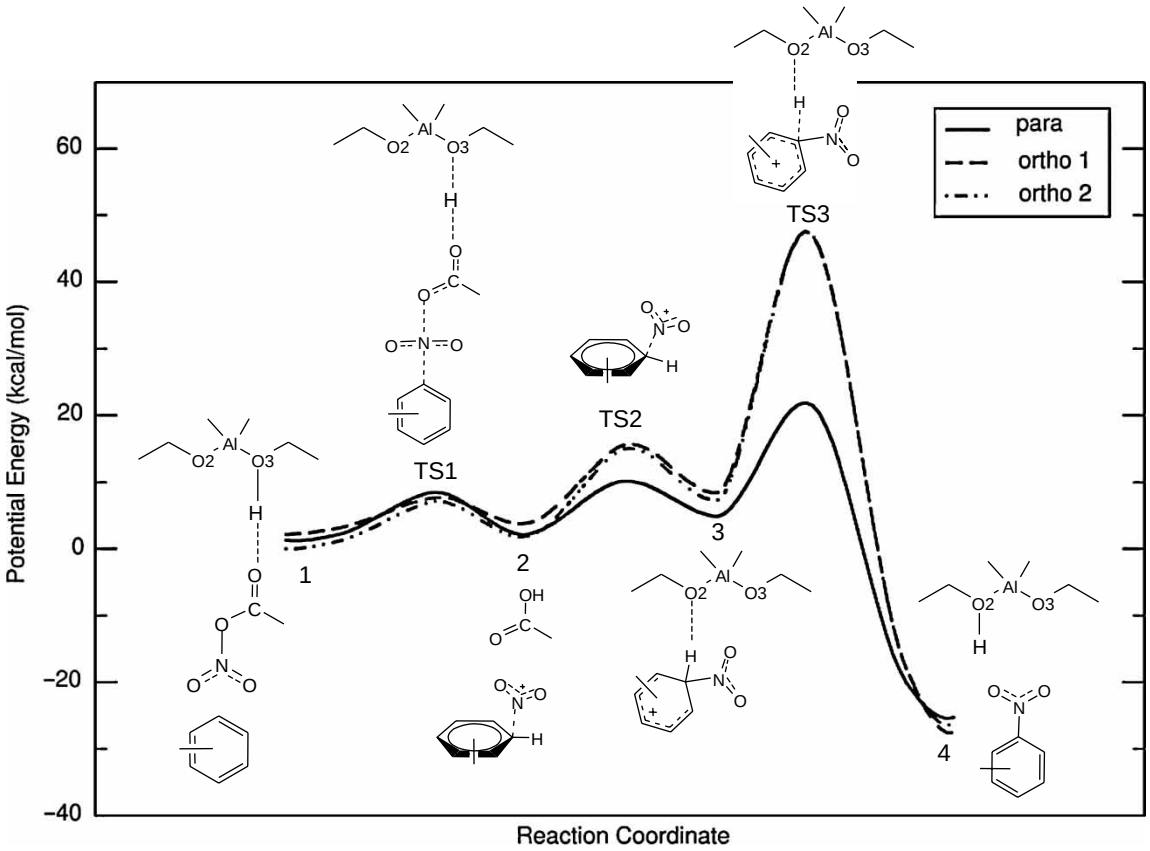

Figure 8. Potential energy plots for the *para* and two *ortho* nitrations according to the calculations done here.

Table 2. Energetics (in kcal/mol) for the *para* and *ortho* electrophilic nitration by acetyl nitrate in the polymorph B H-beta structure at the acid site.

Attack site	*para*	*ortho* 1	*ortho* 2
Reaction energetics			
1 → 2	1.0	1.6	−0.9
2 → 3	2.7	4.5	5.6
3 → 4	−30.3	−36.0	−33.5
Transition state barriers			
1 → TS1	7.2	5.4	4.4
2 → TS2	7.8	11.5	13.0
3 → TS3	16.6	38.9	40.0

See Figure 8 for corresponding product, intermediate and transition states.

transition state for the *para* and two *ortho* nitration scenarios, and Figure 10 shows the structures of the optimised π-complex intermediates for the *para* and two *ortho* nitration scenarios. The C—N distance in the three π-complexes of our calculations are between the 1.997 and 2.434 Å values reported by Esteves et al. for the addition of NO_2^+ to benzene with two different NO_2^+ rotamer configurations in the gas phase calculated at the DFT-B3LYP/6-31++G** level of theory [40]. Figure 8 shows that the addition of a 'nitronium' moiety to the toluene system from the acetyl nitrate is almost the same for all three nitration site scenarios and requires little energy.

However, the second step where the π-complex converts to a σ-complex appears to be energetically prohibitive for the *ortho* nitration scenarios compared with the *para* nitration scenario. The barrier to $\pi-\sigma$ conversion is 4–5 kcal/mol for *para* nitration compared with the two *ortho* nitration scenarios. The *para* nitration reaction for the $\pi-\sigma$ shift is 2–3 kcal/mol more exothermic compared with the two *ortho* nitration cases. Figure 11 shows the transition state structures for the *para* and two *ortho* nitration scenarios. The reason for this difference between the *para* and *ortho* cases is likely due to an increased steric hindrance between the toluene methyl moiety and the zeolite pore wall in the *ortho* cases. In Figure 12, the *para* nitration intermediate (Figure 12(a)) is closer to the closest open acid site (Al1–O2) with the sp^3 hydrogen of the σ-complex at the *para* site 0.350 Å closer than that of the

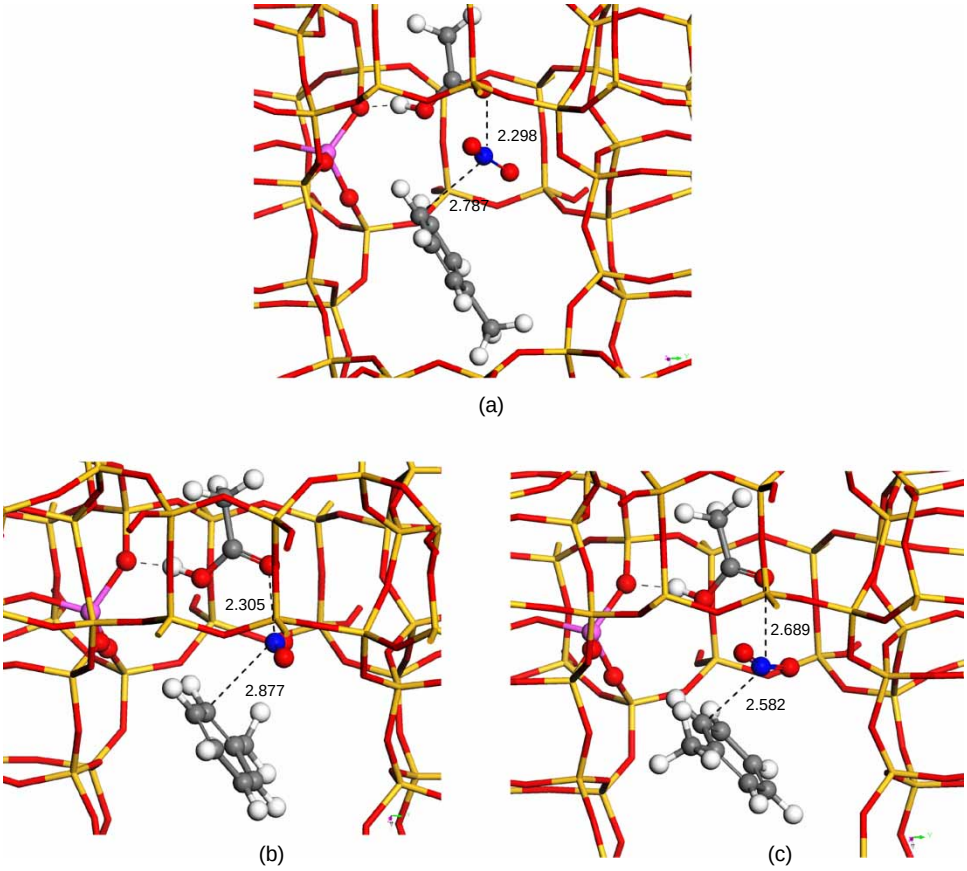

Figure 9. The transition state for the 'nitronium' transfer from the acetyl nitrate to the toluene π-system for (a) *para*, (b) *ortho* 1 and (c) *ortho* 2 attack. Distances and bond lengths are in Angstrom.

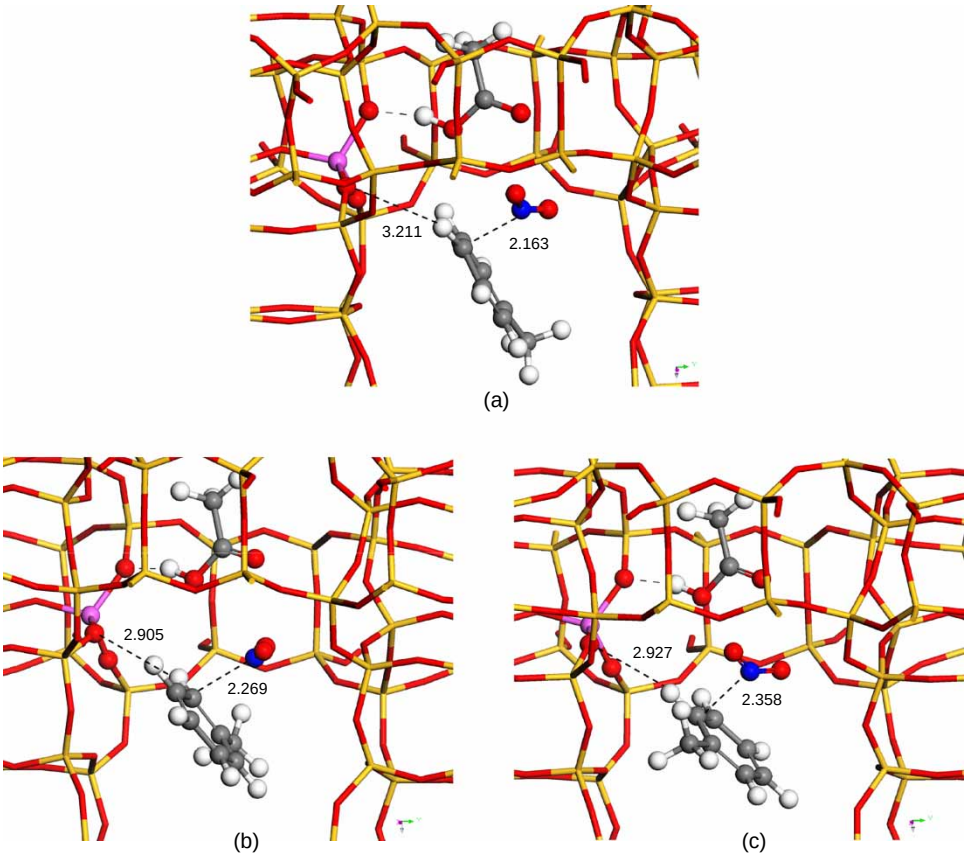

Figure 10. The π-complex for the (a) *para*, (b) *ortho* 1 and (c) *ortho* 2 attack. Distances and bond lengths are in Angstrom.

ortho 1 nitration case (Figure 12(b)) and 0.267 Å closer than that of the *ortho* 2 nitration case (Figure 12(c)). Moreover, the C—N bond length of the σ-complex is shorter in the *para* case by 0.157 and 0.016 Å compared with the *ortho* 1 and *ortho* 2 nitration cases, respectively. These observations from Figure 12(a) to (c) suggest that the σ-complex requires stabilisation by the closest open acid site (Al1–O2) of the zeolite pore wall, and the methyl moiety of the toluene hinders this stabilisation in the two *ortho* site nitration scenarios. The C—N distances in the three σ-complexes of our calculations are in reasonable agreement with the 1.512, 1.587 and 1.747 Å values reported by Esteves et al. for the addition of NO_2^+ to benzene with three different NO_2^+ rotamer configurations in the gas phase calculated at the DFT-B3LYP/6-31++G** level of theory [40].

The steric hindrance of the methyl moiety of the toluene for the *ortho* site nitration is even more profound in the final reaction with the transfer of the sp^3 hydrogen of the σ-complex to the open acid site of the zeolite cage (Al1–O2). This final step has a barrier to reaction that is 22–23 kcal/mol higher in the *ortho* cases compared to that of the *para* case. However, the reaction is 4–6 kcal/mol more exothermic in the *ortho* cases compared with the *para* case. Figure 13 shows the distances that the transferring 'proton' is from open acid site (Al1–O2) and the nitration site of the toluene in each of the transition state structures of the three nitration scenarios (the final product structures are shown in Figure 14). As expected, the distances for the 'proton' in the *para* case are noticeably shorter compared with that of the *ortho* scenarios (by 0.145 and 0.426 Å for the H–O2(Al1) distance in the *ortho* 1 and *ortho* 2 cases, respectively and 0.140 and 0.296 Å for the H—C in the *ortho* 1 and *ortho* 2 cases, respectively). This is suggestive that the steric hindrance of the methyl moiety of the toluene in the *ortho* nitration cases is making the 'proton' transfer of the final step difficult compared with the *para* nitration case. From our analysis, it appears that *ortho* nitration of toluene becomes increasingly difficult with the second step (conversion from the π- to σ-complex) and third step ('proton' transfer from nitration site to the open acid site in the zeolite pore wall) primarily because of the toluene methyl-zeolite pore wall steric hindrance. Our mechanism appears to be at odds with the mechanism Prins and coworkers proposed (illustrated in Figure 1) to explain H-beta's *para*-selective nitration of toluene [14]. They

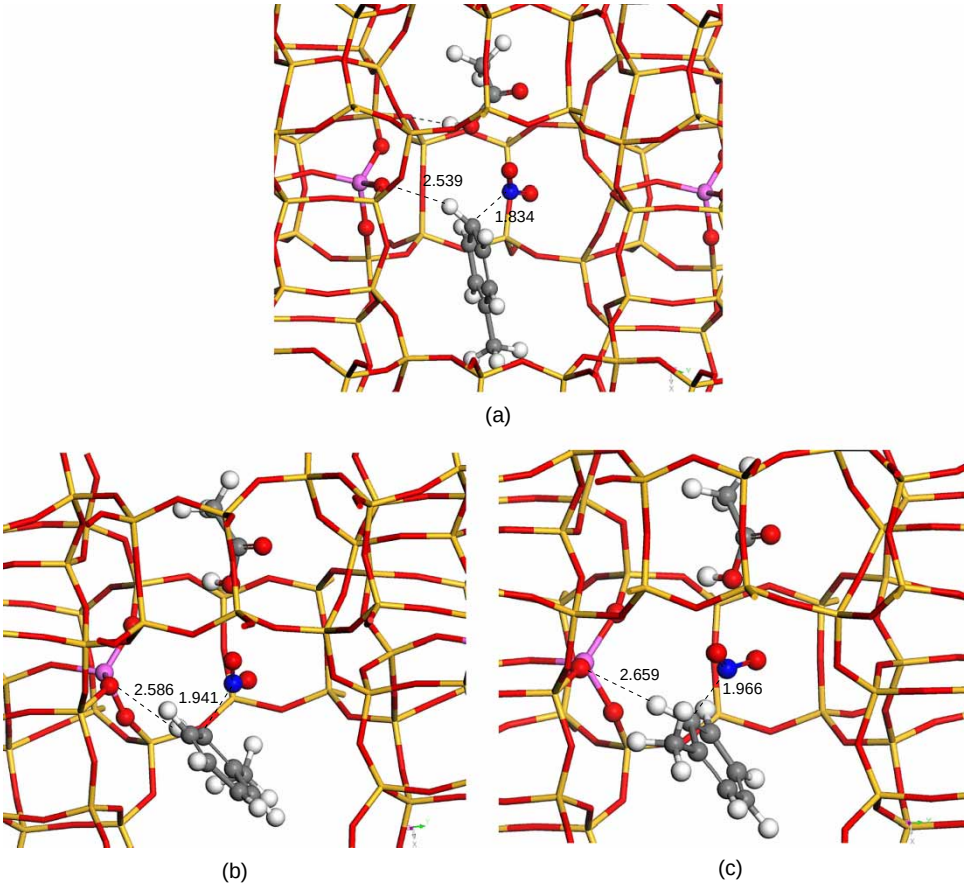

Figure 11. The transition state from the π-complex to the σ-complex for (a) *para*, (b) *ortho* 1 and (c) *ortho* 2 attack. Distances and bond lengths are in Angstrom.

propose that the acetyl methyl group provides the steric hindrance required for the *para* selectivity and not the zeolite pore walls. Conceivably, chemical kinetics experiments exploring the isotopic effect of deuterated H-beta could be used to give credence to the mechanism presented here.

4. Conclusion

Through DFT calculations, we have explored the likely Brønsted acid sites of H-beta polymorph B and applied this work to exploring the origin of H-beta's propensity toward high *para* selection in the nitration of toluene by acetyl nitrate. According to our calculations assuming a single Brønsted acid site, the likely mode of binding of the acetyl nitrate is via the carbonyl oxygen of the acetyl moiety, rather than via octahedral coordination of Al with two nitrate oxygens or the ester linkage oxygen between the acetyl and nitrate moieties. A stable octahedral coordination of the Al was not found with the theory methods used here, and the ester linkage oxygen interaction with the acid site proton was weaker than that of the carbonyl interaction. Moreover, the carbonyl interaction with the cage proton resulted in a longer O—N bond at the ester linkage compared with that of the ester linkage oxygen interaction. This suggests a more labile NO_2^+ moiety for electrophilic attack of the toluene π-system.

With this mode of acetyl nitrate interaction with the acid site proton, further calculations were done to determine stable minima and transition states for the nitration of toluene at the *para* site and both of the *ortho* sites. While the energetics suggest that addition of the 'nitronium' moiety to the toluene to form a 'π-complex' appears to be equally likely at all three electrophilic attack sites, the stabilisation of the 'σ-complex' and the subsequent proton transfer to a zeolite acid site to ultimately form nitrotoluene is more favourable in the *para* attack case than it is for either of the two *ortho* attack cases. In the *ortho* attack cases, steric hindrance caused by the interaction of the methyl group of the toluene with the wall of the zeolite 12-T pore system appears to prevent the stabilisation of the σ-complex slightly and the final transfer of the complex's proton

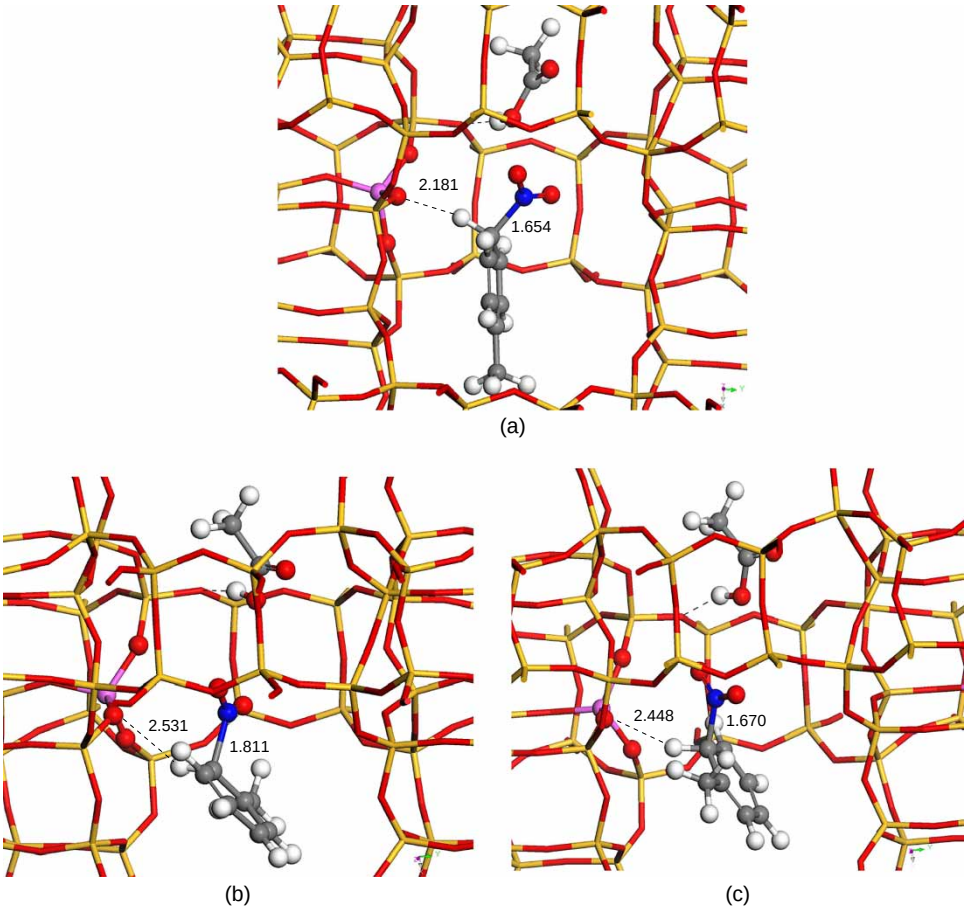

Figure 12. The σ-complex for (a) *para*, (b) *ortho* 1 and (c) *ortho* 2 attack. Distances and bond lengths are in Angstrom.

to one of the acid site oxygens greatly (the barrier to reaction in either of the *ortho* cases is nearly 2.5 times greater than that of the *para* case). With this, we have shown that a more likely mechanism for the *para* selectivity in beta zeolite involves the steric hindrance of the toluene methyl moiety with the zeolite cage wall, not steric hindrance from the acetyl methyl moiety as suggested by Prins and coworkers.

We also acknowledge that the favourable diffusion within microcrystalline beta and the highly flexible framework of beta as well as an appropriate Si/Al ratio (e.g. $\sim$13) and distribution of Al sites must also be partially credited with this zeolite's selective nature in the nitration of monosubstituted benzene compounds. Evidence for this has been provided by the work of Prins and coworkers who have shown a decrease in selectivity upon considerable dealumination (i.e. decrease in acid sites to give a high Si/Al ratio) of beta [16]. The favourable diffusion provided by the large 12-T pore channels allows for transport of the reagents to the internal acid sites and for transport of the products out of the pore system. The flexible framework possibly allows for prolonged sequestering of the nitrate ions at the Lewis acid sites (i.e. effectively trapping nitrate ions at octahedral aluminum acid sites). This may allow for creation of the acetyl nitrate close to the internal acid sites for subsequent reaction with toluene. The flexible acid sites may also create traps for acetic acid species (cage-bound acetate ions at octahedral Lewis acid aluminum sites and cage-bound protons at nearby Brønsted acid sites) that prevent protons from participating in non-selective nitration through homogeneous free acid species in the large pore channels. Prins and coworkers very briefly mentioned that trapping of acetic acid by-product may lead to selectivity but did not give any mechanism on how this may lead to selectivity [14]. We believe that the dual Lewis and Brønsted acid character of many aluminum sites in beta may lead to anchoring both the acetate anion and the proton from acetic acid on to the cage structure. With very few or no 'free' acetic acid protons in the spacious 12-T channels, there is very little unselective solution phase proton transfer from unbound acetic acid taking place. Thus, only heterogeneous proton transfer with the zeolite cage can take place, which is where our mechanism for sterically-restrictive selectivity comes into play. We will

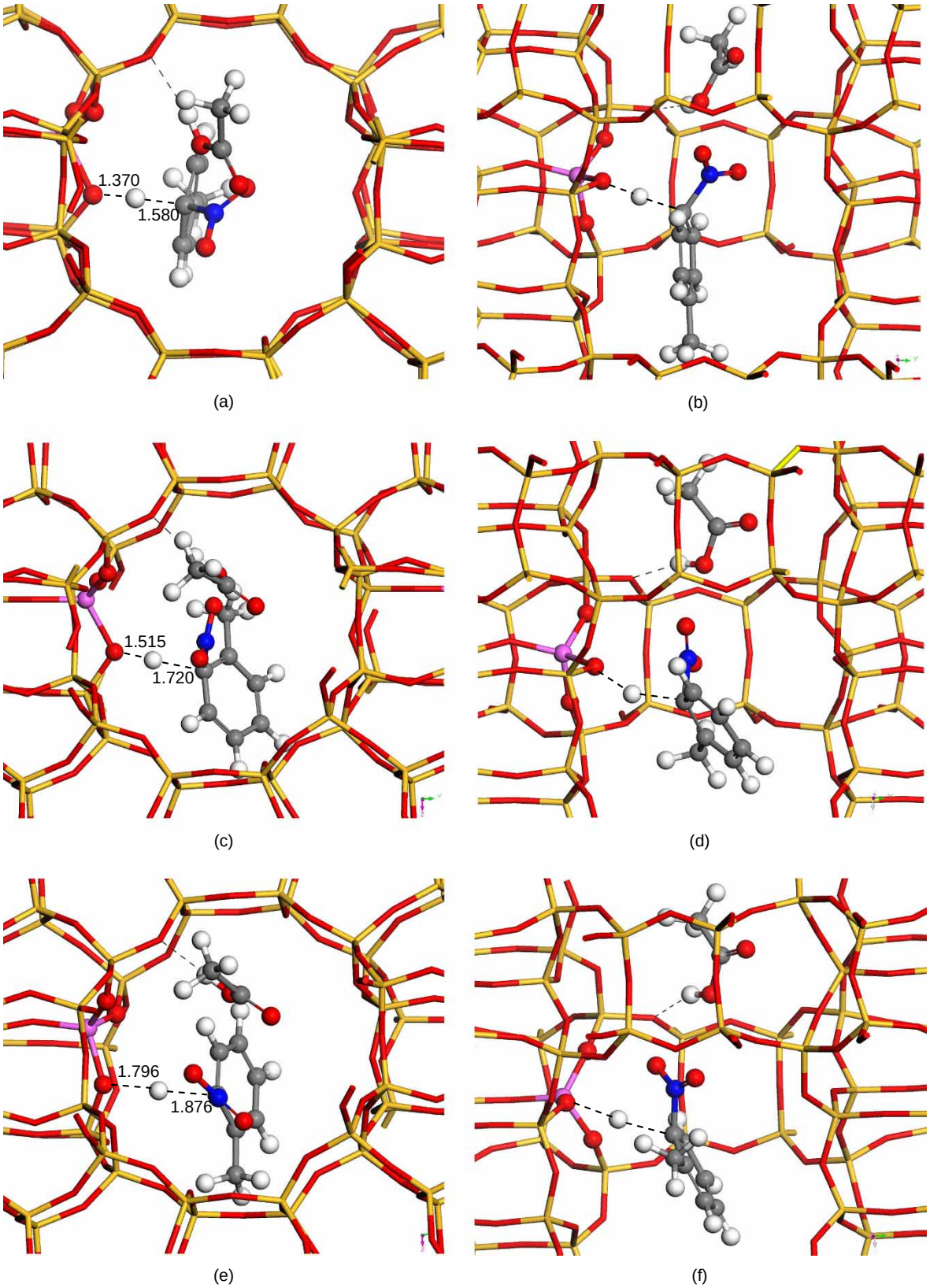

Figure 13. TS3 for *para* nitration (a) viewing down the 12-T pore and (b) viewing a side cross-section of the 12-T pore, *ortho* 1 nitration (c) viewing down the 12-T pore and (d) viewing a side cross-section of the 12-T pore and *ortho* 2 nitration (e) viewing down the 12-T pore and (f) viewing a side cross-section of the 12-T pore. Distances shown are in Angstroms.

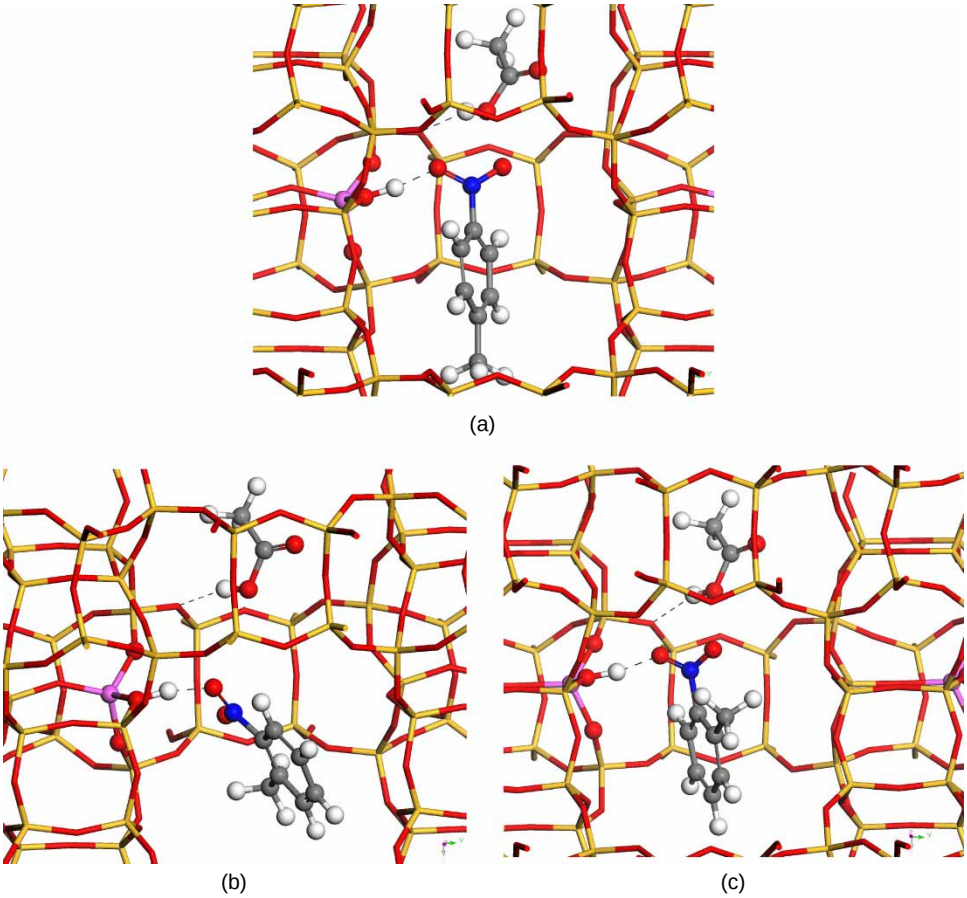

Figure 14. The nitration product resulting from (a) *para*, (b) *ortho* 1 and (c) *ortho* 2 attack.

be exploring this in our future work on this elusive zeolite system.

Acknowledgements

The authors thank Accelrys for the computational resources to perform this work. J.T. Hynes is also acknowledged for his comments regarding potential hydrogen isotopic experiments that could be explored to determine the validity of our mechanism.

References

[1] G.A. Olah, R. Malhotra, and S.C. Narang, *Nitration: Methods and Mechanisms*, VCH, New York, 1989.
[2] K. Schofield, *Aromatic Nitration*, Cambridge University Press, Cambridge, 1980.
[3] R. Taylor, *Electrophilic Aromatic Substitution*, John Wiley, Chichester, 1990.
[4] K.S. Smith, A. Musson, and G.A. DeBoos, *A novel method for the nitration of simple aromatic compounds*, J. Org. Chem. 63 (1998), pp. 8448–8454.
[5] L.G. Wade, *Organic Chemistry*, 3rd ed., Prentice-Hall, Englewood Cliffs, NJ, 1995.
[6] F.J. Waller, A.G.M. Barrett, D.C. Braddock, and D. Ramprasad, *Lanthanide(III) triflates as recyclable catalysts for atom economic aromatic nitration*, Chem. Commun. (1997), pp. 613–614.
[7] G.A. Olah, R. Malhotra, and S.C. Narang, *Aromatic substitution. 43. perfluorinated resinsulfonic acid catalyzed nitration of aromatics*, J. Org. Chem. 43 (1978), pp. 4628–4630.
[8] H.A. Muathen, *Selective nitration of aromatic compounds with bismuth subnitrate and thionyl chloride*, Molecules 8 (2003), pp. 593–598.
[9] A. Cornélis, L. Delaude, A. Gerstmans, and P. Laszlo, *A procedure for quantitative regioselective nitration of aromatic hydrocarbons in the laboratory*, Tetrahedron Lett. 29 (1988), pp. 5909–5912.
[10] K. Smith, K. Fry, M. Butters, and B. Nay, *Para-selective mononitration of alkylbenzene under mild conditions by use of benzoyl nitrate in the presence of a zeolite catalyst*, Tetrahedron Lett. 30 (1989), pp. 5333–5336.
[11] S.M. Nagy, K.A. Yarovoy, M.M. Shakirov, V.G. Shubin, L.A. Vostrikova, and K.G. Ione, *Nitration of aromatic compounds with benzoyl nitrate on zeolites*, J. Mol. Catal. 64 (1991), p. L31.
[12] T.J. Kwok, K. Jayasuriya, R. Damavaparu, and B.W. Brodman, *Application of H-ZSM-5 zeolite for regioselective mononitration of toluene*, J. Org. Chem. 59 (1994), pp. 4939–4942.
[13] T. Esakkidurai, M. Kumarraja, and K. Pitchumani, *Regioselective nitration of aromatic substrates in zeolite cage*, Proc. Indian Acad. Sci. 115 (2003), pp. 113–121.
[14] M. Haouas, S. Bernasconi, A. Kogelbauer, and R. Prins, *An NMR study of the nitration of toluene over zeolites by HNO_3-Ac_2O*, Phys. Chem. Chem. Phys. 3 (2001), pp. 5067–5075.
[15] S. Bernasconi, *Liquid phase nitration of toluene and 2-nitrotoluene using acetyl nitrate: zeolite BEA as para-selective catalyst*, Ph.D. thesis, Swiss Federal Institute of Technology, Zurich, 2003.

[16] S. Bernasconi, G.D. Pirngruber, and R. Prins, *Influence of the properties of zeolite BEA on its performance in the nitration of toluene and nitrotoluene*, J. Catal. 224 (2004), pp. 297–303.

[17] J.A. van Bokhoven, D.C. Koningsberger, P. Kunkeler, H. van Bekkum, and A.P.M. Kentgens, *Stepwise dealumination of zeolite beta at specific T-sites observed with ^{27}Al MAS and ^{27}Al MQ MAS NMR*, J. Am. Chem. Soc. 122 (2000), pp. 12842–12847.

[18] M. Haouas, A. Kogelbauer, and R. Prins, *The effect of flexible lattice aluminium in zeolite beta during the nitration of toluene with nitric acid and acetic anhydride*, Catal. Lett. 70 (2000), pp. 61–65.

[19] A. Abraham, S.-H. Lee, C.-H. Shin, S.B. Hong, R. Prins, and J.A. van Bokhoven, *Influence of framework silicon to aluminium ratio on aluminium coordination and distribution in zeolite beta investigated by ^{27}Al MAS and ^{27}Al MQ MAS NMR*, Phys. Chem. Chem. Phys. 6 (2004), pp. 3031–3036.

[20] J.A. van Bokhoven, A.M.J. van der Eerden, and D.C. Koningsberger, *Three-coordinate aluminum in zeolites observed with* in situ *x-ray absorption near-edge spectroscopy at the Al K-edge: Flexibility of aluminum coordinations in zeolites*, J. Am. Chem. Soc. 125 (2003), pp. 7435–7442.

[21] J.A. van Bokhoven, D.C. Koningsberger, P. Kunkeler, and H. van Bekkum, *Influence of steam activation on pore structure and acidity of zeolite beta: an Al K edge XANES study of aluminum coordination*, J. Catal. 211 (2002), pp. 540–547.

[22] A. Omegna, J.A. van Bokhoven, and R. Prins, *Flexible aluminum coordination in alumino-silicates structure of zeolite H-USY and amorphous silica-alumina amorphous silica-alumina*, J. Phys. Chem. B 107 (2003), pp. 8854–8860.

[23] A. Omegna, M. Haouas, A. Kogelbauer, and R. Prins, *Realumination of dealuminated HZSM-5 zeolites by acid treatment: a re-examination*, Microporous and Mesoporous Mater. 46 (2001), pp. 177–184.

[24] A. Omegna, M. Vasic, J.A. van Bokhoven, G. Pirngruber, and R. Prin, *Dealumination and realumination of microcrystalline zeolite beta: an XRD, FTIR and quantitative multinuclear (MQ) MAS NMR study*, Phys. Chem. Chem. Phys. 6 (2004), pp. 447–452.

[25] A. Omegna, R. Prins, and J.A. van Bokhoven, *Effect of temperature on aluminum coordination in zeolites H-Y and H-USY and amorphous silica-alumina: an* in situ *Al K edge XANES study*, J. Phys. Chem. B 109 (2005), pp. 9280–9283.

[26] C. Jia, P. Massiani, and D. Barthomeuf, *Characterization by infrared and nuclear magnetic resonance spectroscopies of calcined beta zeolite*, J. Chem. Soc. Faraday Trans. 89 (1993), pp. 3659–3665.

[27] S. Bernasconi, G.D. Pirngruber, A. Kogelbauer, and R. Prins, *Factors determining the suitability of zeolite BEA as para-selective nitration catalyst*, J. Catal. 219 (2003), pp. 231–241.

[28] *Materials Studio, Version 4.0*. Three-dimensional graphical images appearing in this work were generated using the Materials Studio visualizer, Accelrys Software, Inc., San Diego, CA, USA, 2005.

[29] B.J. Delley, *An all-electron method for solving the local density functional for polyatomic molecules*, J. Chem. Phys. 92 (1990), pp. 508–517.

[30] B.J. Delley, *From molecules to solids with the DMol^3 approach*, J. Chem. Phys. 113 (2000), pp. 7756–7764.

[31] J.P. Perdew, K. Burke, and M. Ernzerhof, *Generalized gradient approximation made simple*, Phys. Rev. Lett. 77 (1996), pp. 3865–3868.

[32] J. Andzelm, R.D. King-Smith, and G. Fitzgerald, *Geometry optimization of solids using delocalized internal coordinates*, Chem. Phys. Lett. 335 (2001), pp. 321–326.

[33] N. Govind, M. Petersen, G. Fitzgerald, D. King-Smith, and J. Andzelm, *A generalized synchronous transit method for transition state location*, Comput. Mater. Sci. 28 (2003), pp. 250–258.

[34] J.M. Newsam, M.M.J. Treacy, W.T. Koetsier, and C.B. de Gruyter, *Structural characterization of zeolite beta*, Proc. R. Soc. Lond. A 420 (1988), pp. 375–409.

[35] B. Mihailova, V. Valtchev, S. Mintova, A.-C. Faust, N. Petkova, and T. Bein, *Interlayer stacking disorder in zeolite beta family: a Raman spectroscopic study*, Phys. Chem. Chem. Phys. 7 (2005), pp. 2756–2763.

[36] A. Corma, M.T. Navarro, F. Rey, J. Rius, and S. Valencia, *Pure polymorph C of zeolite beta synthesized by using framework isomorphous substitution as a structure-directing mechanism*, Angew. Chem. Int. Ed. 40 (2001), pp. 2277–2280.

[37] J.C. Jansen, E.J. Creyghton, S.L. Njo, H. van Koningsveld, and H. van Bekkum, *On the remarkable behavior of zeolite beta in acid catalysis*, Catal. Today 38 (1997), pp. 205–212.

[38] J. Hill, C.M. Freeman, and B. Delley, *Bridging hydroxyl groups in faujasite: periodic vs cluster density functional calculations*, J. Phys. Chem. A 103 (1999), pp. 3772–3777.

[39] N. Govind, J. Andzelm, K. Reindel, and G. Fitzgerald, *Zeolite-catalyzed hydrocarbon formation from methanol: density functional simulations*, Intl. J. Mol. Sci. 3 (2002), pp. 423–434.

[40] P.M. Esteves, J.W. de M. Carneiro, S.P. Cardoso, A.G.H. Barbosa, K.K. Laali, G. Rasul, G.K.S. Prakash, and G.A. Olah, *Unified mechanistic concept of electrophilic aromatic nitration: convergence of computational results and experimental data*, J. Am. Chem. Soc. 125 (2003), pp. 4836–4849.

[41] A.M. Silva and M.A.C. Nascimento, *A DFT study of nitration of benzene by acyl nitrate catalyzed by zeolites*, Chem. Phys. Lett. 393 (2004), pp. 173–178.

[42] I. Pápai, A. Goursot, F. Fajula, and J. Weber, *Density functional calculations on model clusters of zeolite-beta*, J. Phys. Chem. 98 (1994), pp. 4654–4659.

[43] H. Fujita, T. Kanougi, and T. Atoguchi, *Distribution of Brønsted acid sites on beta zeolite H-BEA: a periodic density functional theory calculation*, Appl. Catal. A: Gen. 313 (2006), pp. 160–166.

[44] C.A. Fyfe, H. Strobl, G.T. Kokotailo, C.T. Pasztor, G.E. Barlow, and S. Bradley, *Correlations between lattice structures of zeolites and their ^{29}Si MAS n.m.r. spectra: zeolites KZ-2, ZSM-12, and beta*, Zeolites 8 (1988), pp. 132–136.

[45] G. Valerio, A. Goursot, R. Vetrivel, O. Malkina, V. Malkin, and D.R. Salahub, *Calculation of ^{29}Si and ^{27}Al MAS NMR chemical shifts in zeolite-beta using density functional theory: correlation with lattice structures*, J. Am. Chem. Soc. 120 (1998), pp. 11426–11431.

[46] W. Löwenstein, *The distribution of aluminum in the tetrahedra of silicates and aluminates*, Am. Mineral. 39 (1954), pp. 92–96.

[47] O. Bortnovsky, Z. Sobalík, and B. Wichterlová, *Exchange of Co(II) ions in H-BEA zeolites: identification of aluminum pairs in the zeolite framework*, Microporous and Mesoporous Mater. 46 (2001), pp. 265–275.

[48] G. Fischer, A. Goursot, B. Coq, G. Delahay, and S. Pal, *Theoretical study of N_2O reduction by Co in Fe-BEA zeolite*, Chem. Phys. Chem. 7 (2006), pp. 1795–1801.

[49] A. Andersen, N. Govind, E.J. Bylaska, in proof. Note: Around the time this work was accepted for publication, our preliminary DFT results show that aluminum sites at the flexible 3–9 positions will not bind with the nitrate moiety of acetyl nitrate to form octahedrally coordinated aluminum. However, nitrate and acetate moieties will bind to these sites to form octahedral aluminum. These promising results further support our mechanism, which does not rely on an Al-bound acetyl nitrate for *para*-selective nitration.